

# A new Multi-Dose Method for extracting source/drain series resistances of halo-doped MOSFETs

Zebang Guo<sup>1</sup>, Zuochang Ye<sup>1</sup>, Xuejie Shi<sup>2</sup>, and Yan Wang<sup>1a)</sup>

<sup>1</sup> Department of Microelectronics and Nanoelectronics, Tsinghua University, Beijing 100084, China

<sup>2</sup> Semiconductor Manufacturing International Corp., Shanghai 201203, China

a) gzb06@mails.tsinghua.edu.cn

**Abstract:** A new method for extracting source/drain series resistances ( $R_{sd}$ ) by combining split-CV and IV data of MOSFETs with multiple halo implant doses (called Multi-Dose Method) is proposed for the first time. This method eliminates the sensitivity of  $R_{sd}$  on effective channel length and considers halo-induced channel resistance increasing. Calibrated TCAD simulation and experimental data of 28-nm bulk MOSFETs with high- $\kappa$  dielectric and metal gates are presented to support and validate the method. The maximum error of this method is within 5%, as compared with 63% for traditional methods. This method has been used as a monitor during technology optimization in foundry.

**Keywords:** source/drain resistances, mobility, MDM, MOSFETs

**Classification:** Electron devices, circuits, and systems

## References

- [1] Y. Taur, C. H. Wann and D. J. Frank: IEDM Tech. Dig. (1998) 789. DOI: [10.1109/IEDM.1998.746474](https://doi.org/10.1109/IEDM.1998.746474)
- [2] K. J. Kuhn: IEEE Trans. Electron Devices **59** (2012) 1813. DOI: [10.1109/TED.2012.2193129](https://doi.org/10.1109/TED.2012.2193129)
- [3] T. Minato and K. Sato: IEICE Electron. Express **11** (2014) 20142002. DOI: [10.1587/elex.11.20142002](https://doi.org/10.1587/elex.11.20142002)
- [4] G. J. Hu, C. Chang and Y. Chia: IEEE Trans. Electron Devices **34** (1987) 2469. DOI: [10.1109/T-ED.1987.23337](https://doi.org/10.1109/T-ED.1987.23337)
- [5] S. Biesemans, M. Hendriks, S. Kubicek and K. D. Meyer: IEEE Trans. Electron Devices **45** (1998) 1310. DOI: [10.1109/16.678555](https://doi.org/10.1109/16.678555)
- [6] Y. H. Chang, Y. F. Wu and C. S. Ho: EDSSC (2007) 87. DOI: [10.1109/EDSSC.2007.4450068](https://doi.org/10.1109/EDSSC.2007.4450068)
- [7] S. Severi, L. Pantisano, E. Augendre, E. S. Andres, P. Eyben and K. D. Meyer: IEEE Trans. Electron Devices **54** (2007) 2690. DOI: [10.1109/TED.2007.904011](https://doi.org/10.1109/TED.2007.904011)
- [8] T. Yuan, D. S. Zicherman, D. R. Lombardi, P. J. Restle, C. H. Hsu, H. I. Hanafi, M. R. Wordeman, B. Davari and G. G. Shahidi: IEEE Electron Device Lett. **13** (1992) 267. DOI: [10.1109/55.145049](https://doi.org/10.1109/55.145049)
- [9] J. P. Campbell, K. P. Cheung, J. S. Suehle and A. Oates: IEEE Electron Device

- Lett. **32** (2011) 1047. DOI:10.1109/LED.2011.2158183
- [10] J. S. Shin, H. Bae, E. Hong, J. Jang, D. Yun, J. Lee, D. H. Kim and D. M. Kim: Solid-State Electron. **72** (2012) 78. DOI:10.1016/j.sse.2012.01.007
- [11] R. D. Pietro, D. Venkateshvaran, A. Klug, E. J. W. List-Kratochvil, A. Facchetti, H. Sirringhaus and D. Neher: Appl. Phys. Lett. **104** (2014) 193501. DOI:10.1063/1.4876057
- [12] S. W. Lee: IEEE Trans. Electron Devices **41** (1994) 403. DOI:10.1109/16.275227
- [13] S. C. Sun and J. D. Plummer: IEEE J. Solid-State Circuits **15** (1980) 562. DOI:10.1109/JSSC.1980.1051439
- [14] D. W. Lin, M. L. Cheng, S. W. Wang, C. C. Wu and M. J. Chen: IEEE Trans. Electron Devices **57** (2010) 890. DOI:10.1109/TED.2010.2041508

## 1 Introduction

With the scaling of MOSFETs, integrated circuits get better performance, lower cost and higher integration density. However, the shrinkage of channel length leads to smaller intrinsic channel resistance ( $R_{ch}$ ), as a result, device performance and circuit delay degradation induced by source/drain series resistances ( $R_{sd}$ ) become more important [1, 2, 3]. Most of  $R_{sd}$  extraction methods are based on the well-known L-array method [4, 5, 6, 7]. These methods have one same assumption: the channel dopant concentration is uniform. In fact, ultra-shallow source/drain (S/D) extensions and halo implants, utilized to control short channel effect, cause the formation of highly nonuniform doped channel and render these methods inadequate. In addition, effective channel length ( $L_{eff}$ ), a key parameter in this technique, is sensitive to gate bias ( $V_g$ ), which brings a vague definition of  $R_{sd}$  and extraction inaccuracy. In recent years, there have been several published  $R_{sd}$  extraction methods aiming at new extraction procedures [8, 9, 10, 11]. However, none of these methods consider the channel nonuniformity.

In this paper, we propose a new  $R_{sd}$  extraction method (called Multi-Dose Method, MDM). Using metallurgical channel length ( $L_{met}$ ) instead of  $L_{eff}$  makes the extraction insensitive to channel length. Halo-induced channel nonuniformity is also considered. These improvements enable one to get accurate  $R_{sd}$ , especially for short-channel MOSFETs with halo implants. Then channel mobility is extracted precisely with accurate  $L_{met}$  and  $R_{sd}$ . MDM is verified by calibrated TCAD simulation and successfully applied to 28 nm experimental MOSFETs.

## 2 Multi-Dose Method

### 2.1 Extraction of $L_{met}$

$L_{eff}$  is defined as the distance between the points where the carrier concentration of lateral S/D diffusion layer becomes equal to that of channel inversion layer.  $L_{met}$  is defined as the distance between source and drain metallurgical junctions.  $L_{eff}$  and  $L_{met}$  are shown in Fig. 1(a).  $L_{eff}$  is susceptible to  $V_g$  while  $L_{met}$  is changelss for a given device.  $L_{met}$  is substituted for  $L_{eff}$  in  $R_{sd}$  extraction for the first time. Therefore, S/D region boundaries are fixed and the dependence of  $R_{sd}$  on channel length is eliminated.

The capacitance-based method [12] provides a way to extract  $L_{\text{met}}$  with split-CV data. Total capacitance between gate and channel ( $C_{\text{gctot}}$ ) contains intrinsic capacitance ( $C_{\text{gc}}$ ), overlap capacitance ( $C_{\text{ov}}$ ), inner and outer fringing capacitance ( $C_{\text{if}}$  and  $C_{\text{of}}$ ) (Fig. 1(b)). In strong inversion region,  $C_{\text{gc}}(V_{\text{ginv}})$  is expressed as

$$C_{\text{gc}}(V_{\text{ginv}}) = C_{\text{gctot}}(V_{\text{ginv}}) - C_{\text{gctot}}(V_{\text{on}}) \quad (1)$$

where  $V_{\text{gon}}$  and  $V_{\text{ginv}}$  stand for turn-on and strong inversion voltage.  $C_{\text{gctot}}(V_{\text{gon}})$  in Eq. (1) represents the sum of parasitic capacitances. Since  $C_{\text{gc}}(V_{\text{ginv}})$  is proportional to  $L_{\text{met}}$ ,  $\Delta L_{\text{met}} (= L_{\text{m}} - L_{\text{met}}, L_{\text{m}}$  is the gate length in mask) can be obtained from the intercept of the  $L_{\text{m}}-C_{\text{gc}}(V_{\text{ginv}})$  curve.

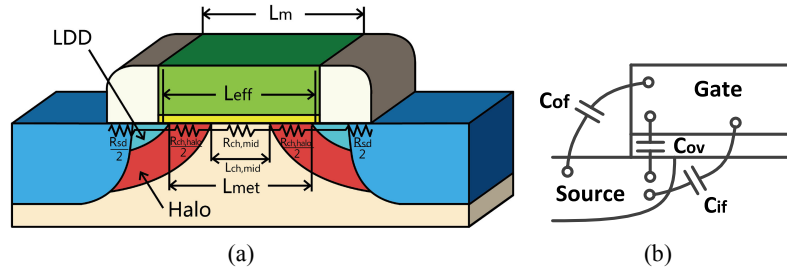


**Fig. 1.** (a) Cross-section view and resistance model (b) capacitance schematic

## 2.2 Halo-induced Channel Resistance Increasing (HCRI)

For the purpose of observing halo induced nonuniform channel, calibrated TCAD simulation is carried out for n-MOSFETs. Fig. 2 displays the internal voltage ( $U_E$ ) of the device along the channel direction. The curve is piecewise linear and the slope can intuitively reflect the value of resistivity. It is obvious that the resistivity of channel in halo region is much bigger than that in middle region.

$R_{\text{ch}}$ , including the channel resistance in middle region and halo region, can be accurately got from TCAD as 330  $\Omega$  (dividing  $U_E$  drop by current). However, traditional methods assume the whole channel is uniformly doped, and extract  $R_{\text{ch}}$  as 229  $\Omega$ . In this condition, HCRI is 101  $\Omega$  (31% increment). Without considering this effect, extraction method would result in enormous error.

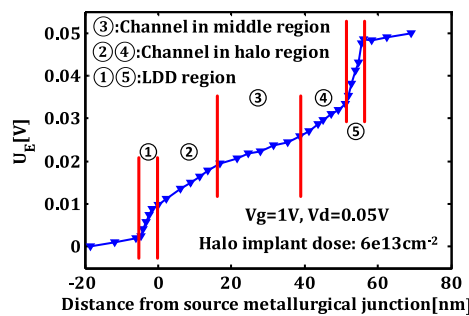


**Fig. 2.** Internal voltage along channel direction

## 2.3 Extraction of $R_{\text{sd}}$

In order to allow for HCRI in  $R_{\text{sd}}$  extraction, we build a new resistance model dividing total resistance ( $R_{\text{tot}}$ ) between source and drain into  $R_{\text{sd}}$ , channel resistance in middle region ( $R_{\text{ch,mid}}$ ) and halo region ( $R_{\text{ch,halo}}$ ) as illustrated in Fig. 1(a). When MOSFET is operating in linear region (drain bias is usually set at 50 mV),  $R_{\text{ch,mid}}$

and  $R_{ch,halo}$  are directly proportional to the lengths of channel in middle region ( $L_{ch,mid}$ ) and halo region ( $L_{ch,halo}$ ) respectively. Consequently,  $R_{tot}$  is described as:

$$\begin{aligned} R_{tot} &= R'_{ch,mid} \cdot L_{ch,mid} + R'_{ch,halo} \cdot L_{ch,halo} + R_{sd} \\ &= (R'_{ch,halo} - R'_{ch,mid}) \cdot L_{ch,halo} + R'_{ch,mid} \cdot L_{met} + R_{sd} \end{aligned} \quad (2)$$

where  $R'_{ch,mid}$  and  $R'_{ch,halo}$  represent average resistance per unit length of channel in middle and halo region, and  $L_{met} = L_{ch,mid} + L_{ch,halo}$ .

To determine  $R'_{ch,mid}$ , currents for multiple MOSFETs with same channel width ( $W$ ) and halo implants but different  $L_m$  are measured.  $L_{ch,halo}$  and  $R_{ch,halo}$  maintain constant. In accordance with Eq. (2),  $R'_{ch,mid}$  can be simply extracted from the slope of the  $L_m$ - $R_{tot}$  curve.

Then, currents for multiple MOSFETs with identical channel doping,  $W$ ,  $L_m$  but different halo implant doses ( $N_{ch,halo}$ ) are measured. For these MOSFETs,  $L_{met}$  and  $L_{ch,halo}$  are assumed to be constant due to rapid thermal annealing in modern CMOS process, and this assumption has been proven in calibrated simulation. Channel resistance is inverse proportional to carrier mobility ( $\mu$ ) and inversion charge ( $Q_{inv}$ ).  $\mu$  decreases with increased doping concentration, which is a result of the increased vertical fields needed to produce surface inversion [13]. When biased in strong inversion with same overdrive voltage ( $V_{gt}$ ), these MOSFETs have identical  $Q_{inv}$ . As a result,  $R'_{ch,mid}$  is invariant and  $R'_{ch,halo}$  is proportional to  $N_{ch,halo}$ .  $N_{ch,halo} = 0$  means  $R'_{ch,halo} = R'_{ch,mid}$ . According to Eq. (2), the  $R_{tot}$ -axis intercept of  $R_{tot}$ - $N_{ch,halo}$  curve is equal to  $R'_{ch,mid} \cdot L_{met} + R_{sd}$ . Finally,  $R_{sd}$  and HCRI are obtained. HCRI is written as

$$HCRI = (R'_{ch,halo} - R'_{ch,mid}) \cdot L_{ch,halo} \quad (3)$$

Without considering HCRI, traditional methods regard the whole channel as uniformly doped and treat  $R'_{ch,mid} \cdot L_{met}$  as  $R_{ch}$ . Therefore HCRI is reckoned into  $R_{sd}$ , leading to overestimation of  $R_{sd}$  and underestimation of  $R_{ch}$ . The proposed method corrects this problem and greatly improves extraction accuracy.

### 3 Experimental results, simulation verification and discussion

#### 3.1 Experimental results

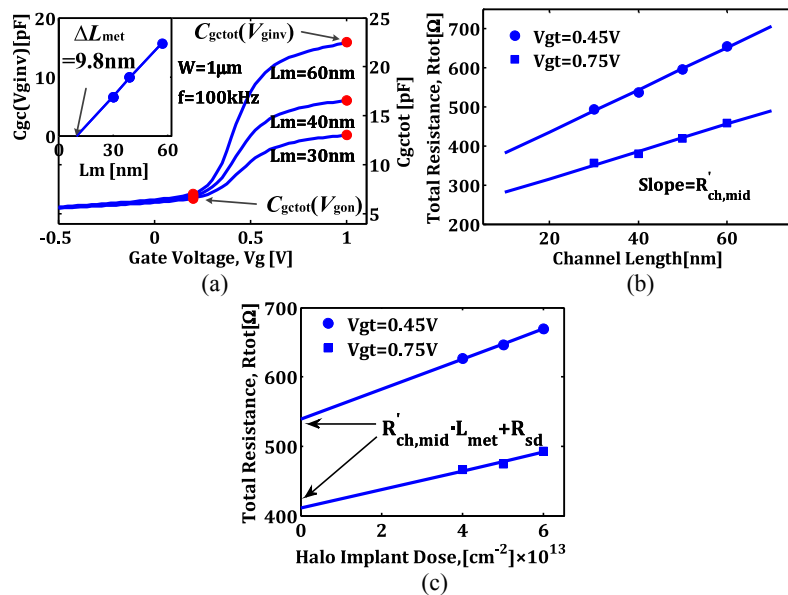


Fig. 3. (a)  $\Delta L_{met}$  extraction (b)  $R_{tot}$ - $L_m$  curve (c)  $R_{tot}$ - $N_{ch,halo}$  curve

The tested devices were fabricated using a 28-nm CMOS process with metal gates and high- $\kappa$  dielectric. The devices have three different halo implants, which are  $4 \times 10^{13}$ ,  $5 \times 10^{13}$  and  $6 \times 10^{13} \text{ cm}^{-2}$  p-type dopant for n-MOSFETs. For each halo implant dose, there are several devices with  $W = 1 \mu\text{m}$  and  $L_m = 30/40/50/60 \text{ nm}$ . Agilent B1500A is used for  $I_d$ - $V_g$  measurement with  $V_d = 50 \text{ mV}$ . Split-CV measurement is executed at 100 kHz by Agilent E4980A.

Taking a device with 30 nm gate length and  $6 \times 10^{13} \text{ cm}^{-2}$  halo implant dose as an example, the extraction procedure are demonstrated in Fig. 3. Firstly, split-CV data are shown in Fig. 3(a).  $C_{\text{gctot}}$  remains independent of channel length until the channel inversion has just started, implying  $V_{\text{gon}}$  is 0.2 V. Then  $\Delta L_{\text{met}}$  is extracted as 9.8 nm (inserted figure), which is well consistent with TEM measurement result. Secondly,  $R_{\text{tot}}$  versus  $L_m$  curve is plotted in Fig. 3(b) and the slope represents  $R'_{\text{ch,mid}}$ . MOSFETs with higher  $V_{\text{gt}}$  have higher carrier concentration, which leads to smaller  $R'_{\text{ch,mid}}$ . Thirdly,  $R_{\text{tot}}$  versus  $N_{\text{ch,halo}}$  curve is plotted in Fig. 3(c). The correlation coefficient between the experimental data and linear regression is above 0.98, indicating  $L_{\text{ch,halo}}$  (slope of  $R_{\text{tot}}$ - $N_{\text{ch,halo}}$ ) keeps constant for different  $N_{\text{ch,halo}}$ . After the above steps, the extraction procedure is completed.

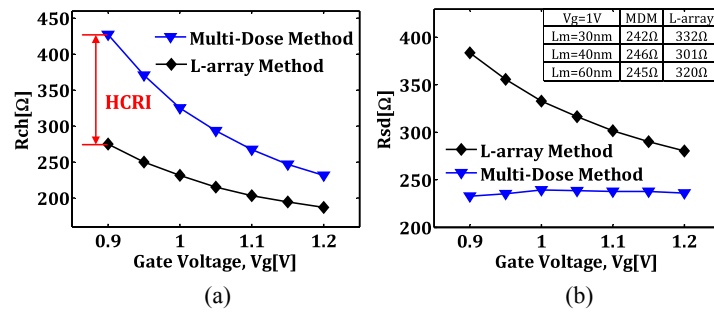


Fig. 4. (a)  $R_{\text{ch}}$  and (b)  $R_{\text{sd}}$  extraction results

As shown in Fig. 4, when devices operate in inversion regime,  $R_{\text{sd}}$  extracted by MDM is holding steady around 240  $\Omega$ . This is reasonable, because  $V_g$  has little effect on modulating carrier concentration and resistance of LDD region in modern MOSFETs (especially in strong inversion) [14]. Conversely,  $R_{\text{sd}}$  extracted by L-array method is strong dependent on  $V_g$  and its dependency relationship is similar with  $R_{\text{ch}}$ . The reason of this phenomenon is that HCRI is reckoned into  $R_{\text{sd}}$  by traditional methods whereas MDM can correct this problem. In addition,  $R_{\text{sd}}$  extracted by MDM is  $L_m$ -independent (inserted table).

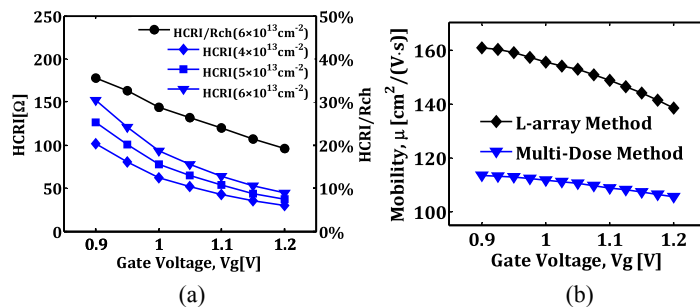


Fig. 5. (a) HCRI and (b) mobility extraction results

Fig. 5(a) elucidates the fact that HCRI is highly significant, as  $HCRI/R_{ch}$  is between 20% and 37%.  $\mu$  can be extracted with accurate  $L_{met}$  and  $R_{sd}$  [7]:

$$\mu = \frac{L_{met} \cdot I_d}{W \cdot Q_{inv} \cdot (V_d - I_d \cdot R_{sd})} \quad (4)$$

$Q_{inv}$  is acquired by integrating  $C_{gc}$ . The result is exhibited in Fig. 5(b).

### 3.2 Simulation results and verification

$R_{sd}$  and  $R_{ch}$  cannot be measured directly in experiment, while they can be obtained precisely by measurement in TCAD simulation. Therefore full process TCAD simulation is carried out to validate our method. In order to be close to the real fabricated devices, the process is the same with technological ones and TCAD simulator is calibrated against experiment. Fig. 6 shows the comparison between experimental and simulated curves of IV and CV characteristics. Excellent agreement is found in the overall operation region.

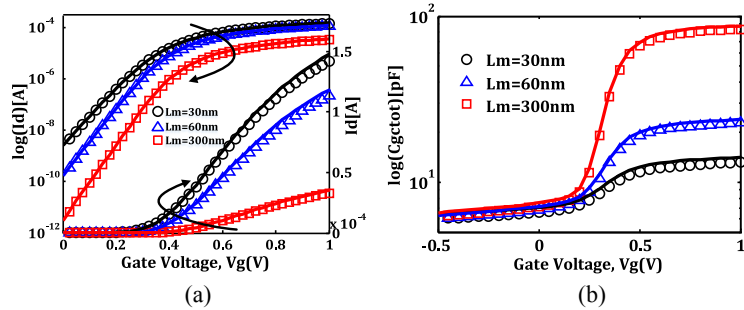


**Fig. 6.** Experimental (symbols) and simulated (lines) curves of (a) IV (b) CV

We can directly observe device sizes, voltages, currents and mobility in TCAD, then real  $L_{met}$ ,  $R_{sd}$ ,  $R_{ch}$  and  $\mu$  can be measured from simulation results precisely. On the other hand, extraction is carried out with simulation data. The extraction errors, which are defined as the difference between the extraction results and TCAD measurement, are shown in Table I. The proposed method is much more accurate than traditional methods.

**Table I.** Maximum extraction error

	this work	from [4]	from [9]	from [10]
$L_{met}$	2%	-	-	-
$R_{sd}$	5%	63%	33%	45%
$R_{ch}$	2%	41%	21%	27%
$\mu$	5%	60%	24%	35%

### 4 Conclusion

This paper presents an efficient and accurate method to extract  $L_{met}$ ,  $R_{sd}$ ,  $R_{ch}$  and  $\mu$ , particularly for short-channel MOSFETs with halo implants. By introducing  $L_{met}$  and considering HCRI, MDM provides immunity against the sensitivity to channel length and exactly separates  $R_{sd}$  and  $R_{ch}$  from  $R_{tot}$ . The validity of MDM is assessed on 28-nm experimental data and calibrated TCAD simulation. Ultimately, MDM is fully compatible with industrial environments and has been employed by foundry to optimize process.